ADVANCES IN ATMOSPHERIC SCIENCES, VOL. 34, MARCH 2017, 289–305

• **Original Paper** •

Changes in Mean and Extreme Temperature and Precipitation over the Arid Region of Northwestern China: Observation and Projection

Yujie WANG[1,4], Botao ZHOU[*2,3], Dahe QIN[2], Jia WU[2], Rong GAO[2], and Lianchun SONG[2]

[1]*School of Atmospheric Sciences, Nanjing University, Nanjing* 210046*, China*
[2]*National Climate Center, China Meteorological Administration, Beijing* 100081*, China*
[3]*Collaborative Innovation Center on Forecast and Evaluation of Meteorological Disasters, Nanjing University of Information Science and Technology, Nanjing* 210044*, China*
[4]*Northwest Climate Center of Gansu Meteorological Bureau, Lanzhou* 730020*, China*

(Received 20 June 2016; revised 18 August 2016; accepted 18 September 2016)

ABSTRACT

This paper reports a comprehensive study on the observed and projected spatiotemporal changes in mean and extreme climate over the arid region of northwestern China, based on gridded observation data and CMIP5 simulations under the RCP4.5 and RCP8.5 scenarios. The observational results reveal an increase in annual mean temperature since 1961, largely attributable to the increase in minimum temperature. The annual mean precipitation also exhibits a significant increasing tendency. The precipitation amount in the most recent decade was greater than in any preceding decade since 1961. Seasonally, the greatest increase in temperature and precipitation appears in winter and in summer, respectively. Widespread significant changes in temperature-related extremes are consistent with warming, with decreases in cold extremes and increases in warm extremes. The warming of the coldest night is greater than that of the warmest day, and changes in cold and warm nights are more evident than for cold and warm days. Extreme precipitation and wet days exhibit an increasing trend, and the maximum number of consecutive dry days shows a tendency toward shorter duration. Multi-model ensemble mean projections indicate an overall continual increase in temperature and precipitation during the 21st century. Decreases in cold extremes, increases in warm extremes, intensification of extreme precipitation, increases in wet days, and decreases in consecutive dry days, are expected under both emissions scenarios, with larger changes corresponding to stronger radiative forcing.

Key words: climate change, arid region, observation, CMIP5 projection

Citation: Wang, Y. J., B. T. Zhou, D. H. Qin, J. Wu, R. Gao, and L. C. Song, 2017: Changes in mean and extreme temperature and precipitation over the arid region of northwestern China: Observation and projection. *Adv. Atmos. Sci.*, **34**(3), 289–305, doi: 10.1007/s00376-016-6160-5.

1. Introduction

The Fifth Assessment Report of the IPCC (2013) indicated that warming of the climate system is unequivocal. The global mean surface temperature has increased at a rate of 0.12°C (10 yr)$^{-1}$ since the 1950s, and changes in many climate extremes have been observed. Continued emissions of greenhouse gases will cause further warming and changes in all components of the climate system, including mean and extreme climate. To better address the changing climate and related climate extremes, regional climate change information is required by the public and policymakers, and is also a major topic of interest in scientific research.

The arid region of northwestern China, including Xinjiang, the Hexi Corridor (Gansu Province), Qaidam Basin (Qinghai Province), the Alashan Plateau (Inner Mongolia), and the northwestern part of Ningxia, is a region with annual mean precipitation of less than 200 mm. This region is also vulnerable to climate change. Because of climate change and sparse vegetation, the ecological systems and water resources of the region are particularly vulnerable (Zhang et al., 2000; Liu et al., 2006). Therefore, it is important to understand present and future climate change in this region, especially changes in climate extremes. Previous studies have documented that the climate over this region has been significantly warming since the second half of the previous century (Ren and Yang, 2006; Li et al., 2014). The extreme minimum and maximum temperatures and the number of extreme precipitation events have also increased (Huang et al., 2014; Shi and Zhao, 2014). Because of global warming and the speeding up of the water cycle, the climate shifted from a warm–dry regime to a warm–humid regime around 1987 (Shi et al., 2002; Song and Zhang, 2003). Based on CMIP3 models and

* Corresponding author: Botao ZHOU
Email: zhoubt@cma.gov.cn

SRES, the climate in the arid region is projected to warm, and the precipitation projected to increase, in the future (e.g., Gao et al., 2003; Xu et al., 2003; Xu et al., 2008; Jiang et al., 2009a; Wu et al., 2011). Similar results have also been projected by regional climate models under the RCP scenarios (Gao et al., 2013; Ji and Kang, 2013a, 2013b).

In recent decades, great progress has been achieved in research on climate extremes. One such effort is that the Expert Team on Climate Change Detection and Indices (ETCCDI) defined a set of climate extreme indices, based on daily temperature and precipitation (Zhang et al., 2011). These indices provide a comprehensive overview of temperature and precipitation statistics, focusing particularly on extreme aspects, and enable changes in global and regional climate extremes to be compared in a standardized way. Another important effort is the development of the CMIP5 modeling framework, which provides coordinated simulations for state-of-the-art global climate models (Taylor et al., 2012). Compared with the CMIP3 framework, CMIP5 features substantial model improvements (Taylor et al., 2012; Xu and Xu, 2012). A number of studies have examined changes in climate extreme indices across different parts of the world in observations (e.g., Alexander et al., 2006; Alexander and Arblaster, 2009; Rusticucci, 2012; Donat et al., 2013; Kruger and Sekele, 2013; Zhou et al., 2016) and projections (e.g., Gao et al., 2006; Tebaldi et al., 2006; Kharin et al., 2007; Alexander and Arblaster, 2009; Xu et al., 2012; Sillmann et al., 2013; Zhou et al., 2014; Ji and Kang, 2015). However, a detailed and comprehensive investigation of changes in mean climate and ETCCDI extreme indices over the arid region of northwestern China is still lacking. How have observations changed, and how will they change in the future as projected by CMIP5 simulations? The present study was conducted to answer these questions.

2. Data and method

The gridded observation dataset named CN05.1 was used in this study, including daily mean temperature, daily maximum temperature, daily minimum temperature, and daily precipitation. The CN05.1 dataset was constructed from observations at 2400 stations across China, and interpolated using the "anomaly approach", i.e., a gridded climatology was first calculated, and then a gridded daily anomaly was added to the climatology to produce the final dataset (Wu and Gao, 2013).

The projected temperature and precipitation data were derived from the outputs of 24 CMIP5 models (ACCESS1.0, BCC_CSM1.1, BNU-ESM, CanESM2, CCSM4, CESM1-BGC, CMCC-CM, CNRM-CM5, CSIRO Mk3.6.0, GFDL-ESM2G, GFDL-ESM2M, HadGEM2-CC, HadGEM2-ES, INM-CM4.0, IPSL-CM5A-LR, IPSL-CM5A-MR, IPSL-CM5B-LR, MIROC5, MIROC-ESM, MIROC-ESM-CHEM, MPI-ESM-LR, MPI-ESM-MR, MRI-CGCM3, NorESM1-M) for the RCP4.5 and RCP8.5 simulations (Taylor et al., 2012). The RCP4.5 and RCP8.5 scenarios, which have radiative forcings peaking at 4.5 W m^{-2} and 8.5 W m^{-2} by 2100, represent the medium-low and high radiative forcing scenarios, respectively. Details on the models and forcings can be found on the CMIP5 website (http://cmip-pcmdi.llnl.gov/cmip5/).

Since the multi-model ensemble mean (MME) has been demonstrated to outperform individual models and is expected to provide more robust estimates of future changes (e.g., Gleckler et al., 2008; Jiang et al., 2009b, 2016; Chen, 2013; Gupta et al., 2013; Sillmann et al., 2013; Zhou et al., 2014), we focus on the projection of the MME, calculated as the arithmetic average of the 24 models. Because the CMIP5 models have different spatial resolutions, data from the different models were interpolated to a common $1^\circ \times 1^\circ$ grid using bilinear interpolation for the MME calculation. The statistical significance was determined using the Student's *t*-test. The climate extreme indices analyzed in this study are summarized in Table 1. Readers are referred to the ETCCDI website (http://etccdi.pacificclimate.org/list_27_indices.shtml) for their definitions and calculation details.

3. Observation

3.1. *Temperature*

Figure 1a shows the spatial distribution of linear trends in annual mean temperature during 1961–2012. The entire arid region has undergone warming since the 1960s, with rapid warming in the western part of Qinghai, the northern part of Xinjiang, the Alashan Plateau of Inner Mongolia, and the northwestern part of Ningxia. Regionally averaged, the annual mean temperature has increased at a rate of 0.31°C (10 yr)$^{-1}$, significant at the 95% level (Fig. 1b). Such an increase may largely stem from the contribution of the increase in annual mean minimum temperature. During the same period, the increasing rate of the annual mean minimum temperature is 0.46°C (10 yr)$^{-1}$, 50% greater than the annual mean temperature. From the seasonal perspective, the mean temperatures in the four seasons all show upward trends, and the warming amplitude is relatively larger in winter [0.41°C (10 yr)$^{-1}$] and autumn [0.34°C (10 yr)$^{-1}$] than in summer [0.26°C (10 yr)$^{-1}$] and spring [0.25°C (10 yr)$^{-1}$] (Figs. 1c–f). The decadal transition from the negative phase to the positive phase also occurs earliest in winter. These observations suggest a large contribution of the winter season to the change in annual mean temperature.

Figure 2 displays temporal changes of temperature extreme indices averaged over the arid region of northwestern China. For the minimum of daily minimum temperature (TNn) (Fig. 2a) and the maximum of daily maximum temperature (TXx) (Fig. 2b), absolute indices describing the coldest night and the hottest day, respectively, a significant increasing trend is clearly apparent during 1961–2012. The respective warming rates for TNn and TXx are 0.43°C (10 yr)$^{-1}$ and 0.17°C (10 yr)$^{-1}$, indicating a greater temperature increase for the coldest night than the warmest day. The warming

Table 1. Information on the climate extreme indices analyzed in the present study.

Abbreviation	Definition and calculation	Category	Units
TNn	Minimum of TN: Let TNn be the daily minimum temperature in month k, period j. The minimum daily minimum temperature each month is then: $\mathrm{TNn}_{kj} = \min(\mathrm{TNn}_{kj})$	Absolute indices	°C
TXx	Maximum of TX: Let TXx be the daily maximum temperatures in month k, period j. The maximum daily maximum temperature each month is then: $\mathrm{TXx}_{kj} = \max(\mathrm{TXx}_{kj})$	Absolute indices	°C
FD	Frost days: Let TN_{ij} be the daily minimum temperature on day i, period j. Count the number of days where $\mathrm{TN}_{ij} < 0$°C	Threshold indices	d
ID	Ice days: Let TX_{ij} be the daily maximum temperature on day i, period j. Count the number of days where $\mathrm{TX}_{ij} < 0$°C	Threshold indices	d
TN10p	Cold nights: Let TN_{ij} be the daily minimum temperature on day i, period j, and let $\mathrm{TN}_{in}10$ be the calendar day 10th percentile centered on a 5-day window for the base period 1961–90. The percentage of days in a year is determined where $\mathrm{TN}_{ij} < \mathrm{TN}_{in}10$	Percentile indices	%
TN90p	Warm nights: Let TN_{ij} be the daily minimum temperature on day i, period j, and let $\mathrm{TN}_{in}90$ be the calendar day 90th percentile centered on a 5-day window for the base period 1961–90. The percentage of days is determined where $\mathrm{TN}_{ij} > \mathrm{TN}_{in}90$	Percentile indices	%
TX10p	Cold days: Let TX_{ij} be the daily maximum temperature on day i, period j, and let $\mathrm{TX}_{in}10$ be the calendar day 10th percentile centered on a 5-day window for the base period 1961–90. The percentage of days is determined where $\mathrm{TX}_{ij} < \mathrm{TX}_{in}10$	Percentile indices	%
TX90p	Warm days: Let TX_{ij} be the daily maximum temperature on day i, period j, and let $\mathrm{TX}_{in}90$ be the calendar day 90th percentile centered on a 5-day window for the base period 1961–90. The percentage of days is determined where $\mathrm{TX}_{ij} > \mathrm{TX}_{in}90$	Percentile indices	%
R95p	Very wet days: Let PR_{wj} be the daily precipitation amount on a wet day w (PR $\geqslant$ 1 mm) in period j, and let $\mathrm{PR}_{wn}95$ be the 95th percentile of precipitation on wet days in the 1961–90 period. If W represents the number of wet days in the period, then: $\mathrm{R95p}_j = \sum_{w=1}^{W} \mathrm{PR}_{wj}$, where $\mathrm{PR}_{wj} > \mathrm{PR}_{wn}95$	Threshold indices	mm
R1mm	Number of wet days: Let PR_{ij} be the daily precipitation amount on day i, period j. Count the number of days where $\mathrm{PR}_{ij} > 1$ mm	Threshold indices	d
CDD	Consecutive dry days: Let PR_{ij} be the daily precipitation amount on day i, period j. Count the largest number of consecutive days where $\mathrm{PR}_{ij} < 1$ mm	Duration indices	d

of TNn is widespread across the arid region. The most significant change occurs at high elevations, such as over the Tianshan Mountains (Fig. 3a). TXx also warms over the entire region, except for some parts of Xinjiang where a slight negative trend is apparent. The warming rate generally increases from west to east, with the greatest increase occurring in Qinghai and Inner Mongolia (Fig. 3b).

Consistent changes can be observed in temperature threshold indices, such as frost days (FD) and ice days (ID) derived from daily minimum temperature and daily maximum temperature, respectively. As shown in Figs. 2c and d, decreases in FD and ID are prevalent during 1961–2012. The decreasing rates are 3.9 d (10 yr)$^{-1}$ for FD and 2.0 d (10 yr)$^{-1}$ for ID. FD decreases everywhere in the arid region, particularly in Qinghai and the high elevations of Xinjiang, such as the Kunlun and Tianshan mountains, where the reduction reaches more than 31 days after 1961 (Fig. 3c). The decrease in ID since 1961 is the largest in Qinghai, with the reduction exceeding 23 days. The smallest decrease is found in Xinjiang. In contrast, there is a slight increase in the Tarim Basin (Fig. 3d).

The temperature percentile indices for the arid region of northwestern China, including warm days (TX90p) and nights (TN90p), based on the upper tail of the maximum and minimum temperature distribution, respectively, and cold days (TX10p) and nights (TN10p), based on the lower tail of the maximum and minimum temperature distribution, respectively, have also exhibited significant changes since the 1960s. As shown in Figs. 2e–h, increases in warm days and nights, concurrent with decreases in cold days and nights, are highly pronounced. The trends are 1.1% (10 yr)$^{-1}$ and 2.3% (10 yr)$^{-1}$ for TX90p and TN90p, respectively (indicative of increasingly more warm days and nights), and −0.6% (10 yr)$^{-1}$ and −1.3% (10 yr)$^{-1}$ for TX10p and TN10p, respectively (indicative of increasingly fewer cold days and nights). Changes in nighttime temperature indices, based on minimum temperature (TN90p and TN10p), are greater than for daytime temperature indices, based on maximum temperature (TX90p and TX10p). Such features of the changes in TX90p and TN90p, as well as TX10p and TN10p, are apparent everywhere across the arid region, with the strongest changes mainly over the southern flank of the region (Figs. 3e–h).

3.2. *Precipitation*

Figure 4a presents the spatial distribution of linear trends in annual mean precipitation during 1961–2012. Clearly, the annual mean precipitation increases across a broad region, with the largest increases appearing in Qinghai and the Tianshan Mountains region. However, it decreases in the western part of Inner Mongolia and the eastern corner of the region. With respect to the regional average, the annual mean precipitation delineates a significant increasing tendency, with a rate of 5.4 mm (10 yr)$^{-1}$. The precipitation amount in the last

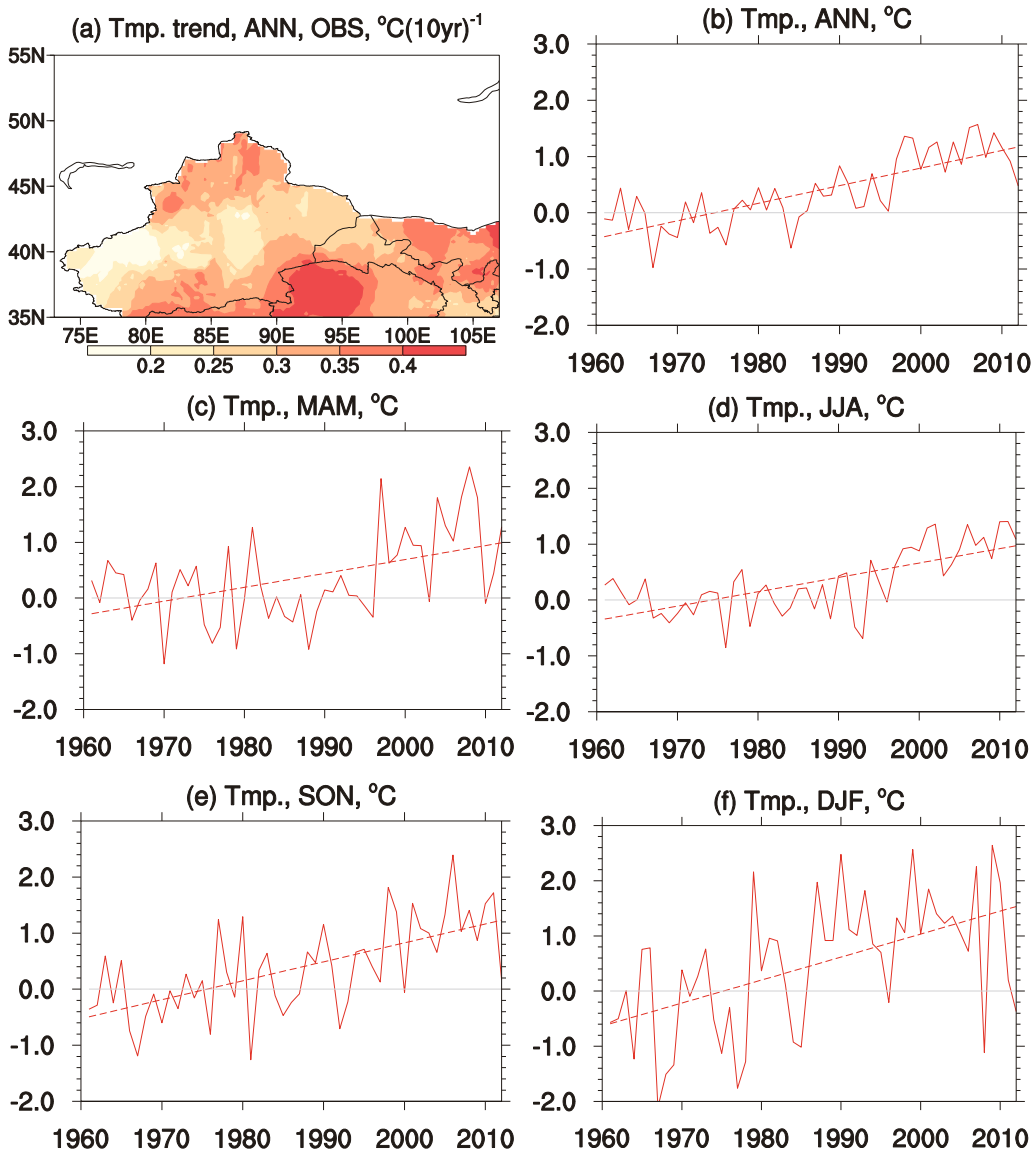

Fig. 1. Spatial distribution of (a) linear trends in annual mean temperature during 1961–2012, and temporal change of the temperature anomaly (relative to 1961–90) averaged over the arid region of northwestern China for (b) the annual mean, (c) spring, (d) summer, (e) autumn and (f) winter. Dashed lines show linear trends.

decade of the century is greater than in any preceding decade since 1961 (Fig. 4b). Seasonal precipitation amounts are all characterized by upward trends (Figs. 4c–f). The rate of increase is largest in the summer season [2.4 mm (10 yr)$^{-1}$], followed by the spring season [1.1 mm (10 yr)$^{-1}$] and the autumn and winter seasons [0.9 mm (10 yr)$^{-1}$].

The spatiotemporal changes in precipitation extreme indices, including the total extremely wet days' total amount (R95p), the number of wet days (R1mm) and the maximum number of consecutive dry days (CDD), are plotted in Fig. 5. For the regional average, both R95p and R1mm show a tendency toward increases in the past 52 years, with rates of 2.4 mm (10 yr)$^{-1}$ and 1.2 d (10 yr)$^{-1}$, respectively (Figs. 5a and b). CDD, a measure of extremely dry conditions, shows a downward trend, with a value of 5.4 d (10 yr)$^{-1}$ (Fig. 5c). In terms of spatial distribution, the changes in R95p and R1mm are generally similar across most regions (Figs. 5d and e); for example, the largest increase is in Qinghai and northwestern Xinjiang; and there is a decrease in western Inner Mongolia and southern Gansu, which indicates that extreme heavy precipitation and precipitation frequency both contribute to increases or decreases in local precipitation. However, in a small region of the Tarim Basin (in Ningxia), the decreasing R95p and increasing R1mm (increasing R95p and decreasing R1mm) imply a larger contribution of precipitation frequency to the enhancement (reduction) of local precipitation amounts. For CDD, there is a tendency toward a shorter duration of dry spells in most of the region, particularly over eastern Xinjiang, western Gansu and northern Qinghai. In contrast, regions such as the western Tarim Basin, central and western Inner Mongolia, and southern Gansu, experience longer durations of dry spells (Fig. 5f).

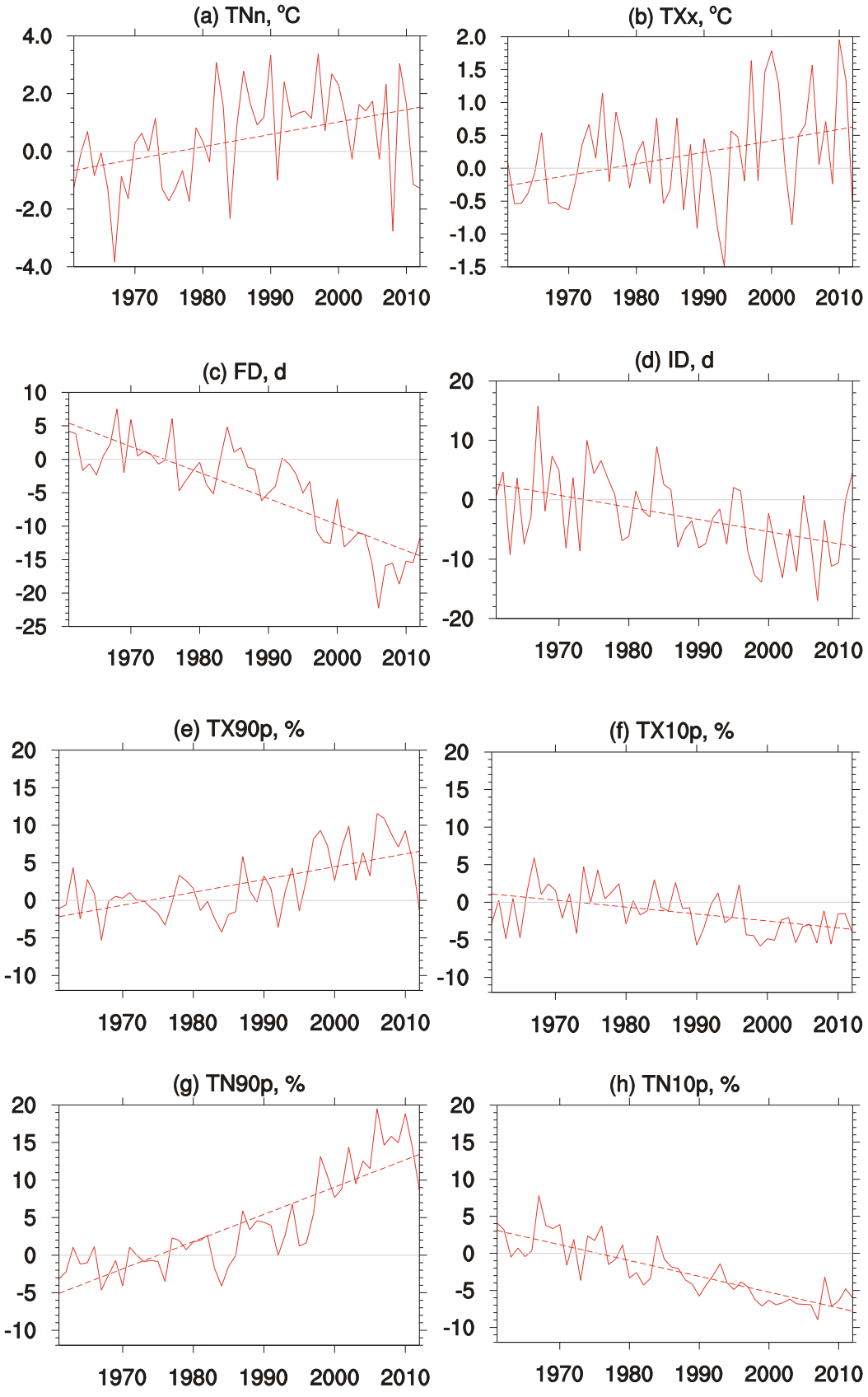

Fig. 2. Temporal change of temperature extreme indices averaged over the arid region of northwestern China. All indices are anomalies relative to 1961–90. Dashed lines show linear trends.

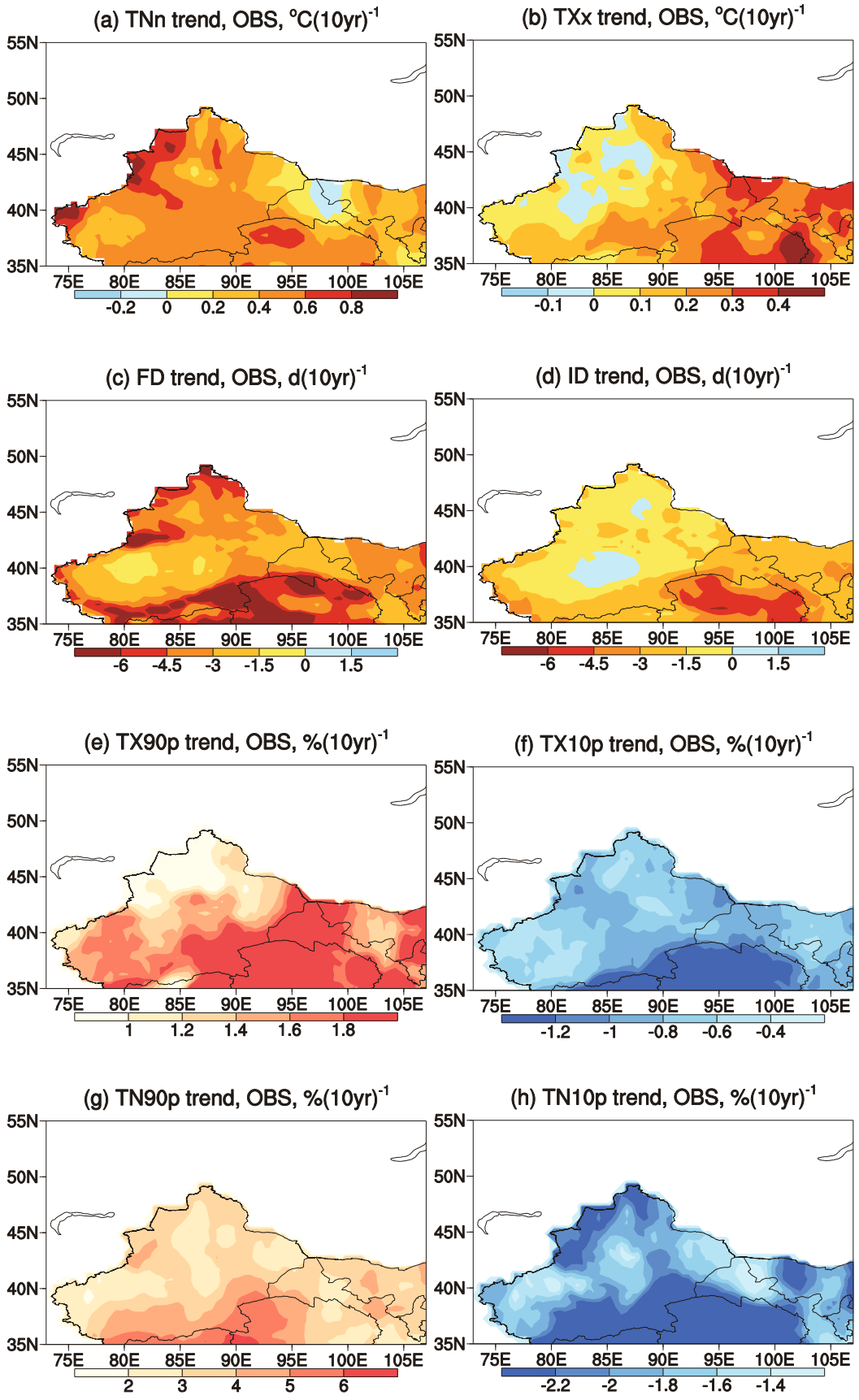

Fig. 3. Spatial distribution of linear trends in temperature extreme indices during 1961–2012.

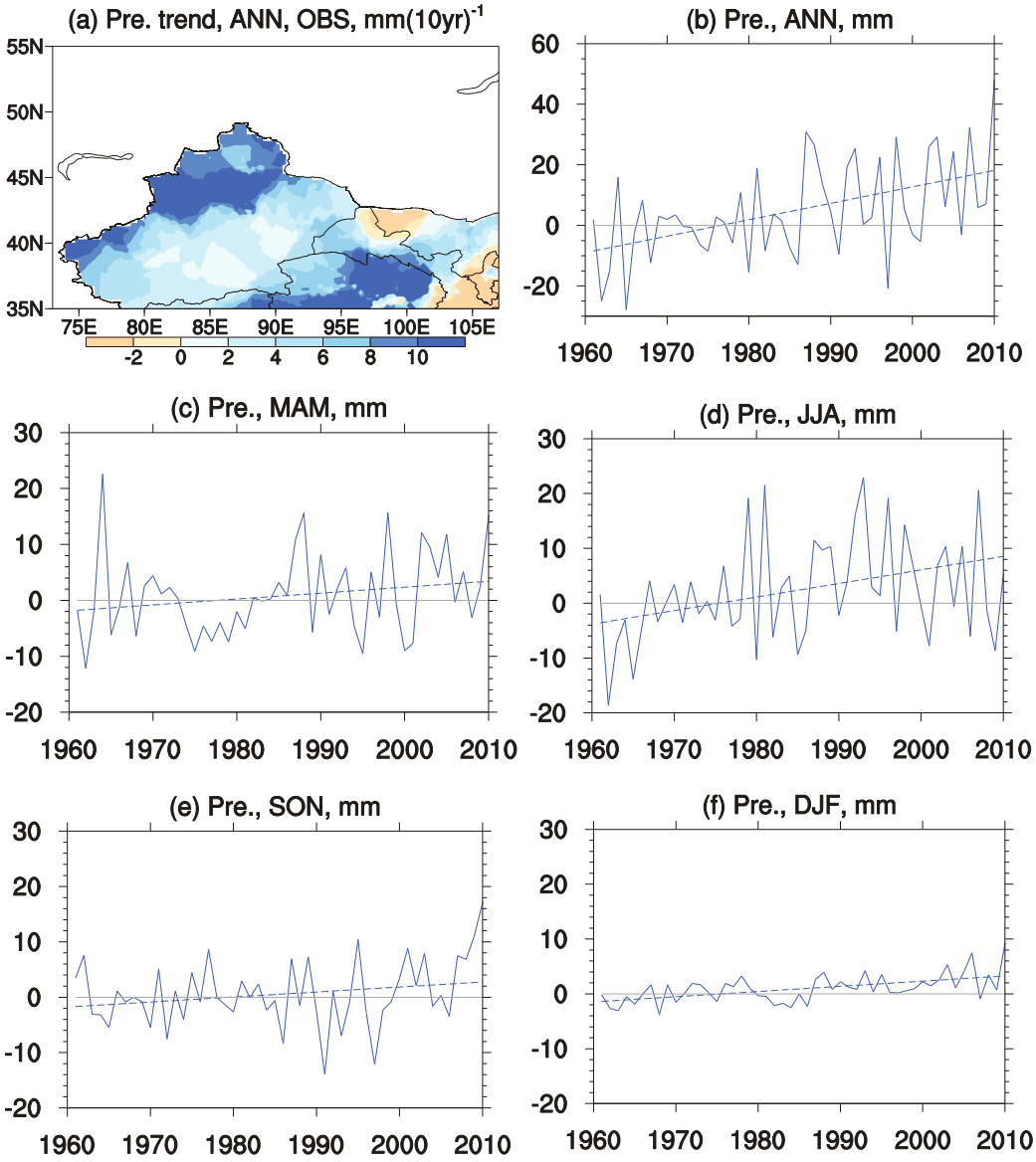

Fig. 4. Spatial distribution of (a) linear trends in annual mean precipitation during 1961–2012, and temporal change of the precipitation anomaly (relative to 1961–90) averaged over the arid region of northwestern China for (b) the annual mean, (c) spring, (d) summer, (e) autumn and (f) winter. Dashed lines show linear trends.

4. Projection

4.1. *Temperature*

The MME projected temporal changes of annual and seasonal mean temperature averaged over the arid region of northwestern China under the RCP4.5 and RCP8.5 scenarios are shown in Figs. 6a1–a5, which indicates an overall upward trend and greater warming under RCP8.5 than RCP4.5, due to stronger external forcing. Under the RCP8.5 (RCP4.5) scenario, the projected rates of annual, spring, summer, autumn and winter temperatures during 2020–99 are 0.68°C, 0.63°C, 0.69°C, 0.69°C and 0.70°C (0.23°C, 0.23°C, 0.23°C, 0.22°C and 0.26°C) per decade, respectively. Relative to the reference period (1986–2005) of the simulation, the annual, spring, summer, autumn and winter temperatures are projected to increase by 2.0°C, 1.9°C, 2.0°C, 2.0°C and 2.0°C (1.6°C, 1.6°C, 1.7°C, 1.6°C and 1.6°C) before the middle of this century (2030–49), and by 5.5°C, 5.2°C, 5.6°C, 5.6°C and 5.6°C (2.6°C, 2.5°C, 2.6°C, 2.6°C and 2.7°C) at the end of this century (2080–99), respectively. Such a warming tendency appears across the arid region. Under the RCP8.5 scenario (Figs. 6c1–c5), a large increase in annual mean temperature occurs mainly in the northern and southern parts of the region. The warming pattern in spring and in winter is similar to that for the annual mean, but the increasing amplitude is weaker in spring and stronger in winter. The warming rate in summer increases from southeast to northwest. In autumn, the largest increase appears along Kunlun Mountains. A roughly similar distribution is seen for RCP4.5 (Figs. 6b1–b5), albeit less remarkable when compared with RCP8.5.

For the absolute indices, significant warming in the regional average is also projected in both TNn (Fig. 7a) and

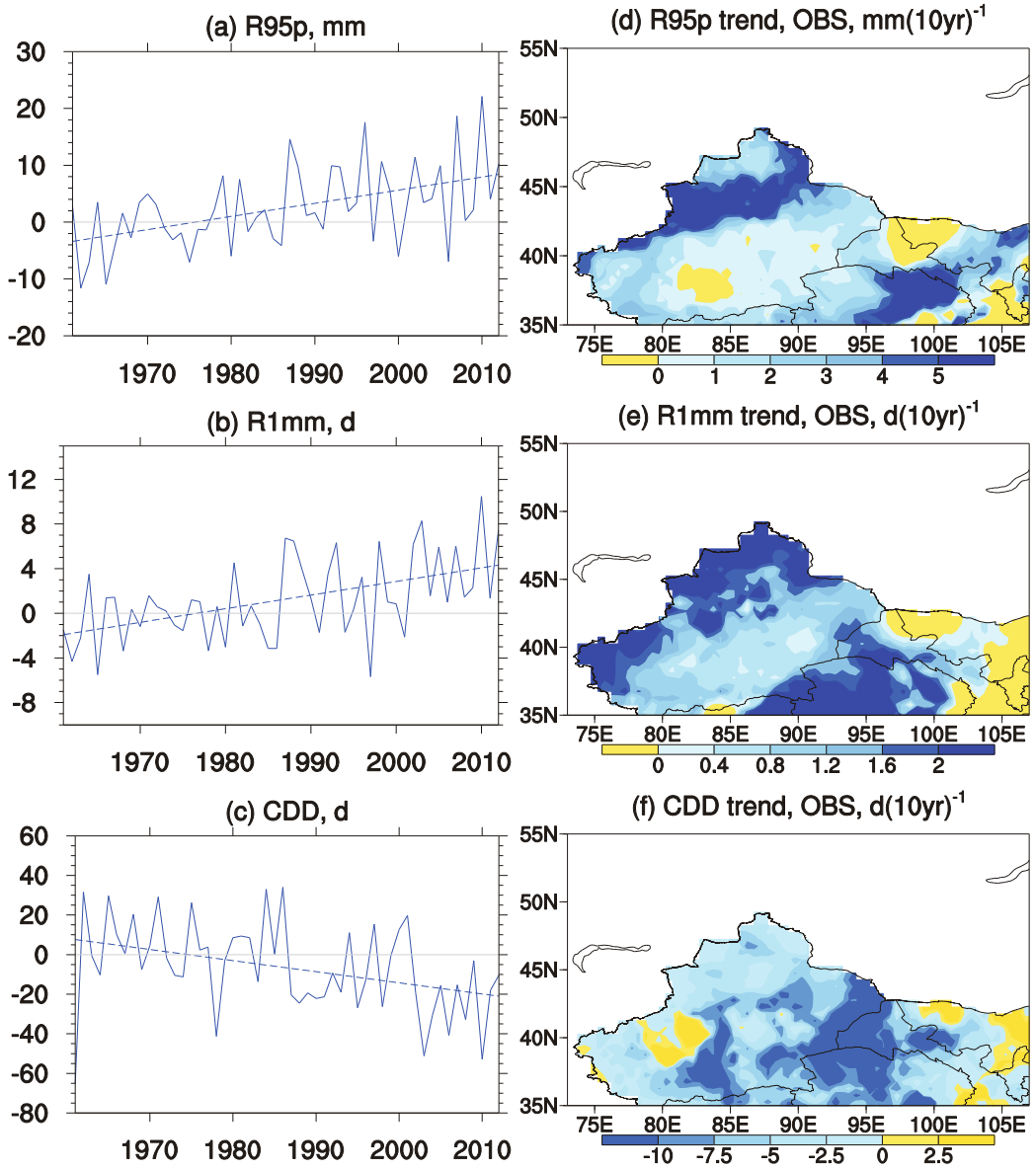

Fig. 5. (a–c) Temporal change of precipitation extreme indices averaged over the arid region of northwestern China. All indices are anomalies relative to 1961–90. Dashed lines show linear trends. (d–f) Spatial distribution of linear trends in precipitation extreme indices during 1961–2012.

TXx (Fig. 7b), with increases in RCP8.5 greater than in RCP4.5, and increases in TNn larger than in TXx. Under the RCP8.5 (RCP4.5) scenario, the warming trends in TNn and TXx during 2020–99 are 0.82°C and 0.71°C (0.32°C and 0.26°C) per decade, respectively. With respect to 1986–2005, the projected increases in TNn and TXx are 2.2°C and 1.9°C (1.7°C and 1.6°C) before the middle of this century, respectively, and the increase is further enhanced to 6.6°C and 5.6°C (3.1°C and 2.8 °C) by the end of this century, respectively.

FD (Fig. 7c) and ID (Fig. 7d) are projected to decrease under both scenarios. The projected decreasing trends in FD and ID from 2020 to 2099 are 2.2 d (10 yr)$^{-1}$ and 2.3 d (10 yr)$^{-1}$, respectively, under the RCP4.5 scenario. Projected changes under the RCP8.5 scenario are much greater, with a reduction of 6.4 d (10 yr)$^{-1}$ for FD and 5.9 d (10 yr)$^{-1}$ for ID. Relative to 1986–2005, FD and ID tend to decrease by 15 days and 13 days under RCP4.5 and by 18 days and 17 days under RCP8.5, respectively, before the middle of this century. By the end of this century, the reduction in FD and ID increases further to 24 days (for both) under RCP4.5, and to 51 days and 47 days under RCP8.5, respectively.

Consistent with warming and projections of the absolute and threshold temperature indices, increases in TX90p (Fig. 7e) and TN90p (Fig. 7g) and decreases in TX10p (Fig. 7f) and TX10p (Fig. 7h) are projected. Relative to 1986–2005, TX90p and TN90p tend to increase by 15.8% and 20.0% (12.0% and 15.3%) before the middle of this century, and by 47.2% and 55.7% (22.4% and 27.6%) at the end of this century, under the RCP8.5 (RCP4.5) scenario, respectively. This result implies an increasing number of warm days and nights in the future, with the change in warm nights stronger than

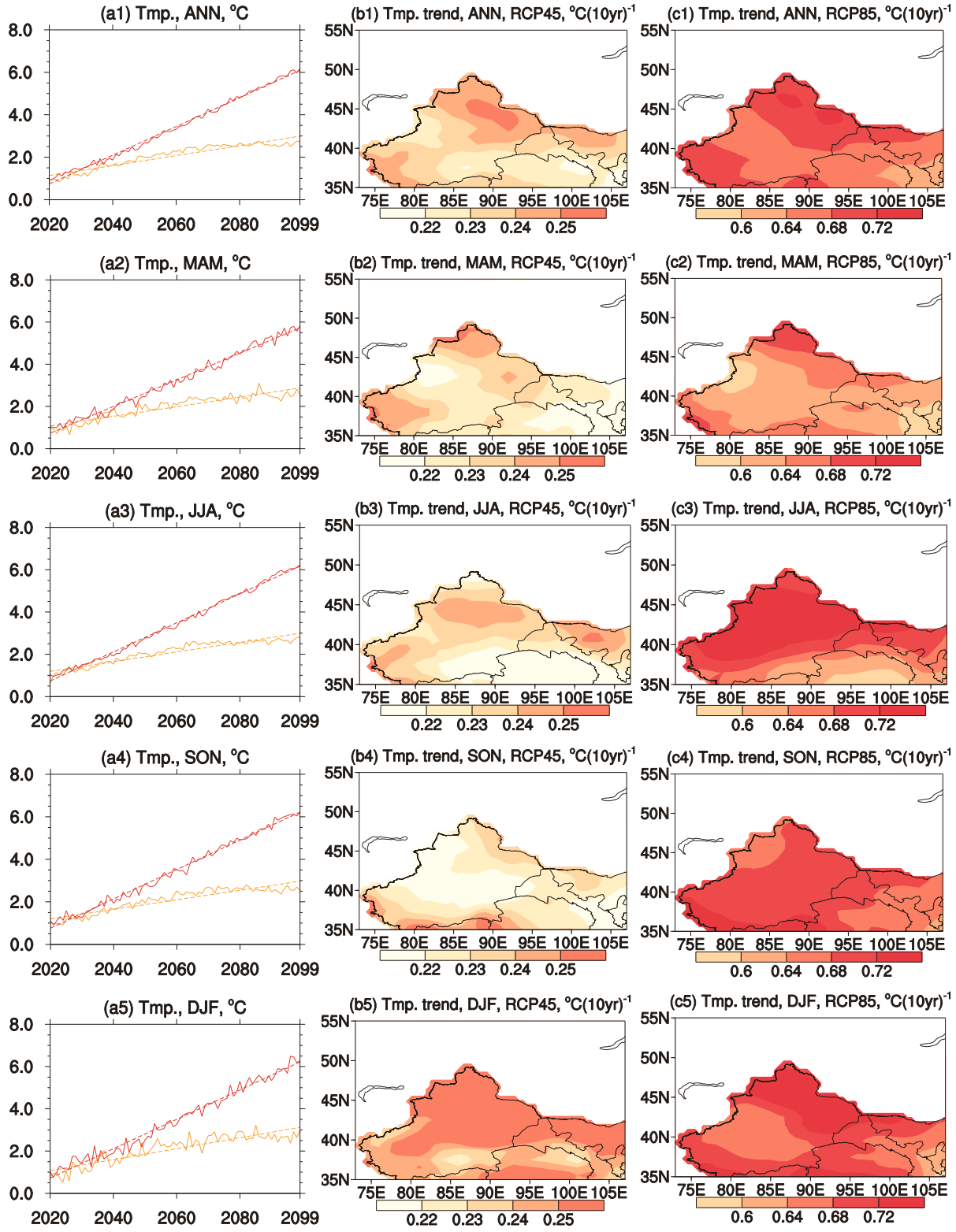

Fig. 6. The MME projected (a1–a5) temporal change of the temperature anomaly (relative to 1986–2005) averaged over the arid region of northwestern China under the RCP4.5 (yellow) and RCP8.5 (red) scenarios, and spatial distribution of linear trends in temperature during 2020–99 under (b1–b5) RCP4.5 and (c1–c5) RCP8.5. Dashed lines show linear trends.

in warm days. The projected changes in TX10p and TN10p are comparable, with a decrease of 4.6% and 5.1% (3.9% and 4.4%) before the middle of this century, and 7.7% and 7.6% (5.6% and 5.9%) at the end of this century, under the RCP8.5 (RCP4.5) scenario, respectively. The indication is that there will be increasingly fewer cold days and nights in the future.

The aforementioned changes are all significant at the 95% level. Additionally, large deviations in changes between

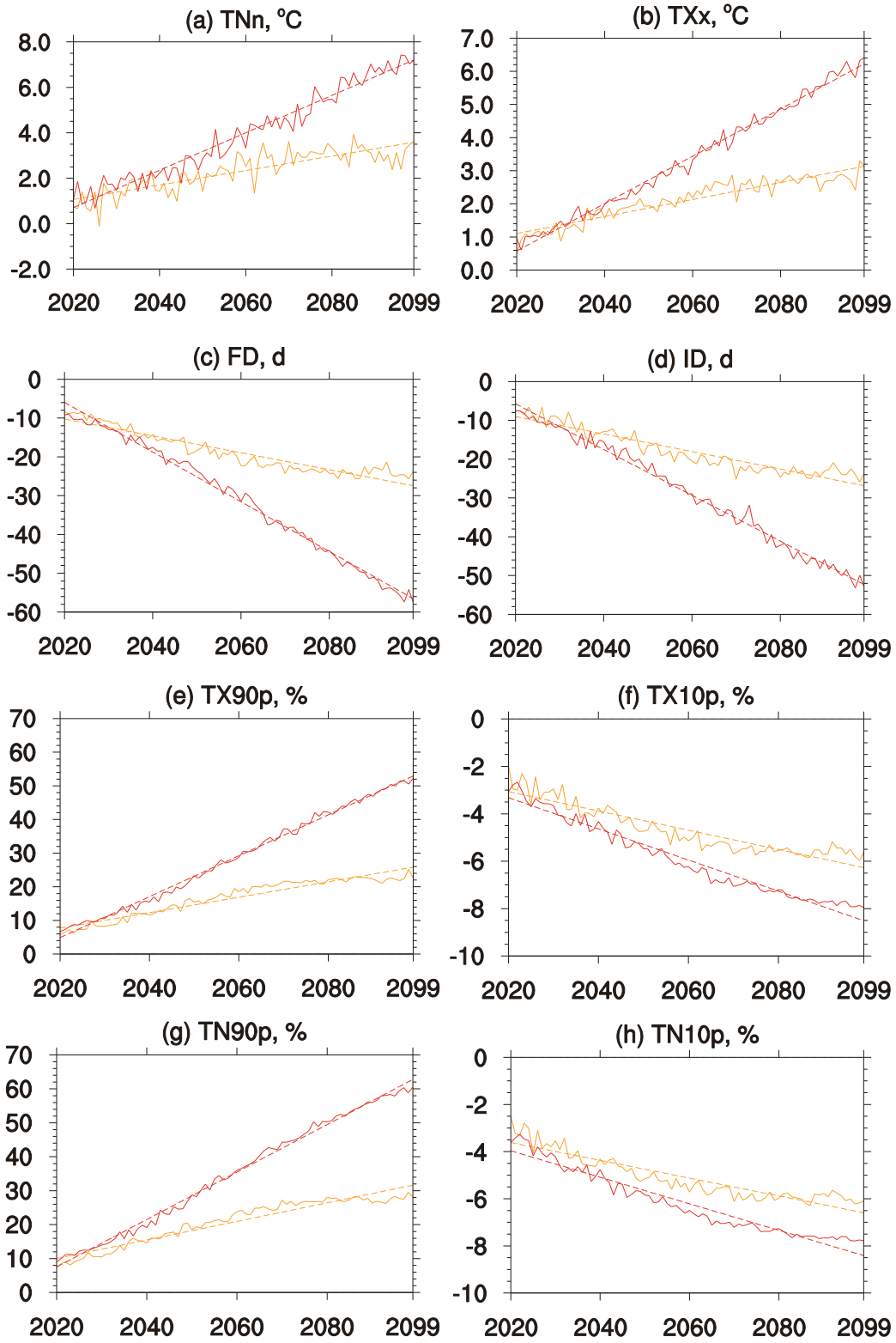

Fig. 7. The MME projected temporal change of temperature extreme indices averaged over the arid region of northwestern China under the RCP4.5 (yellow) and RCP8.5 (red) scenarios. All indices are anomalies relative to 1986–2005. Dashed lines show linear trends.

RCP8.5 and RCP4.5 appear after the 2040s, which demonstrates that the impact of different scenarios on the temperature and temperature-related indices will be very little before that time.

Figures 8 and 9 further present the spatial distribution of linear trends of temperature extreme indices during 2020–99 under the RCP4.5 and RCP8.5 scenarios, respectively. The entire region is projected to undergo consistent changes. Un-

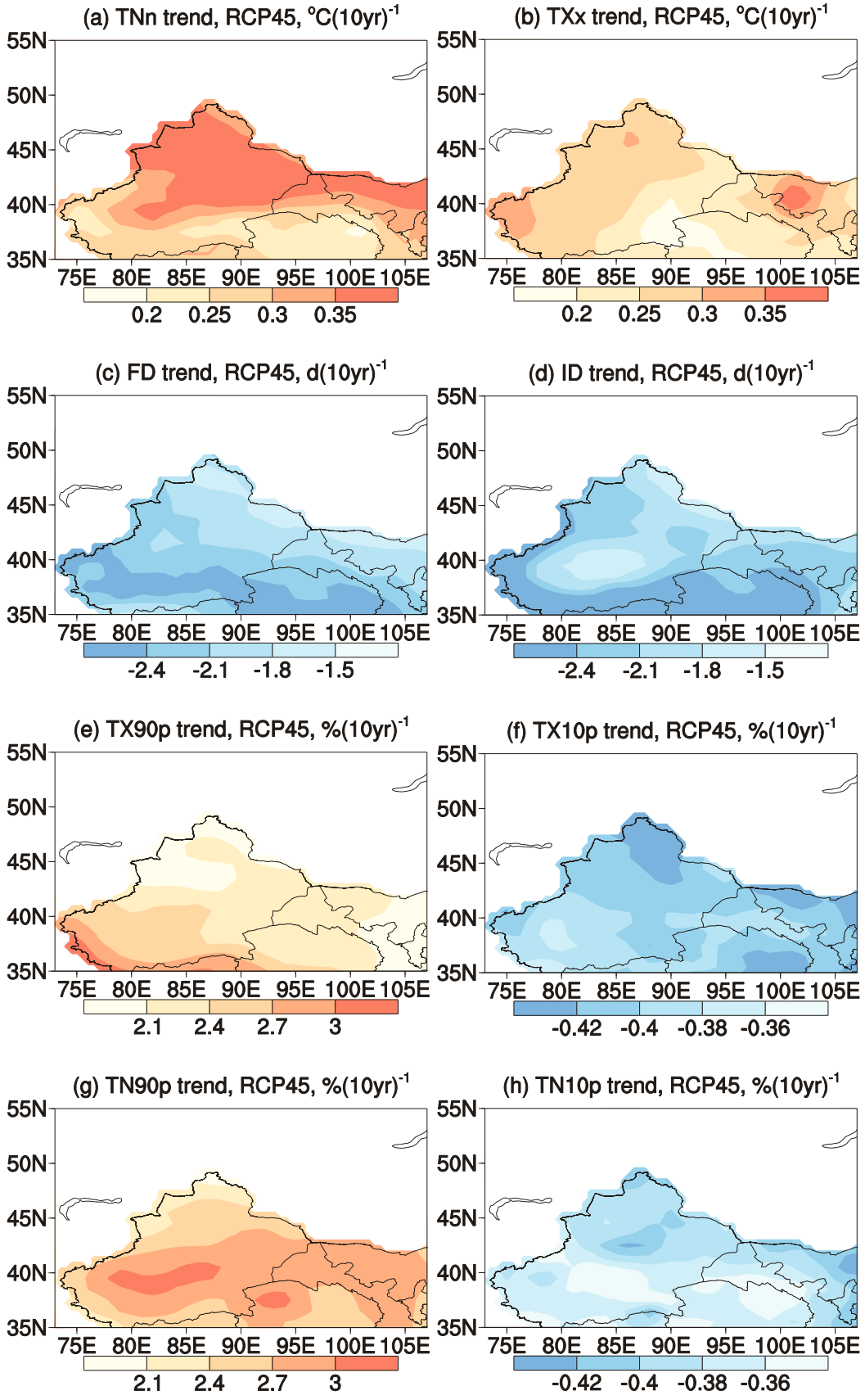

Fig. 8. The MME projected distribution of linear trends in temperature during 2020–99 under the RCP4.5 scenario.

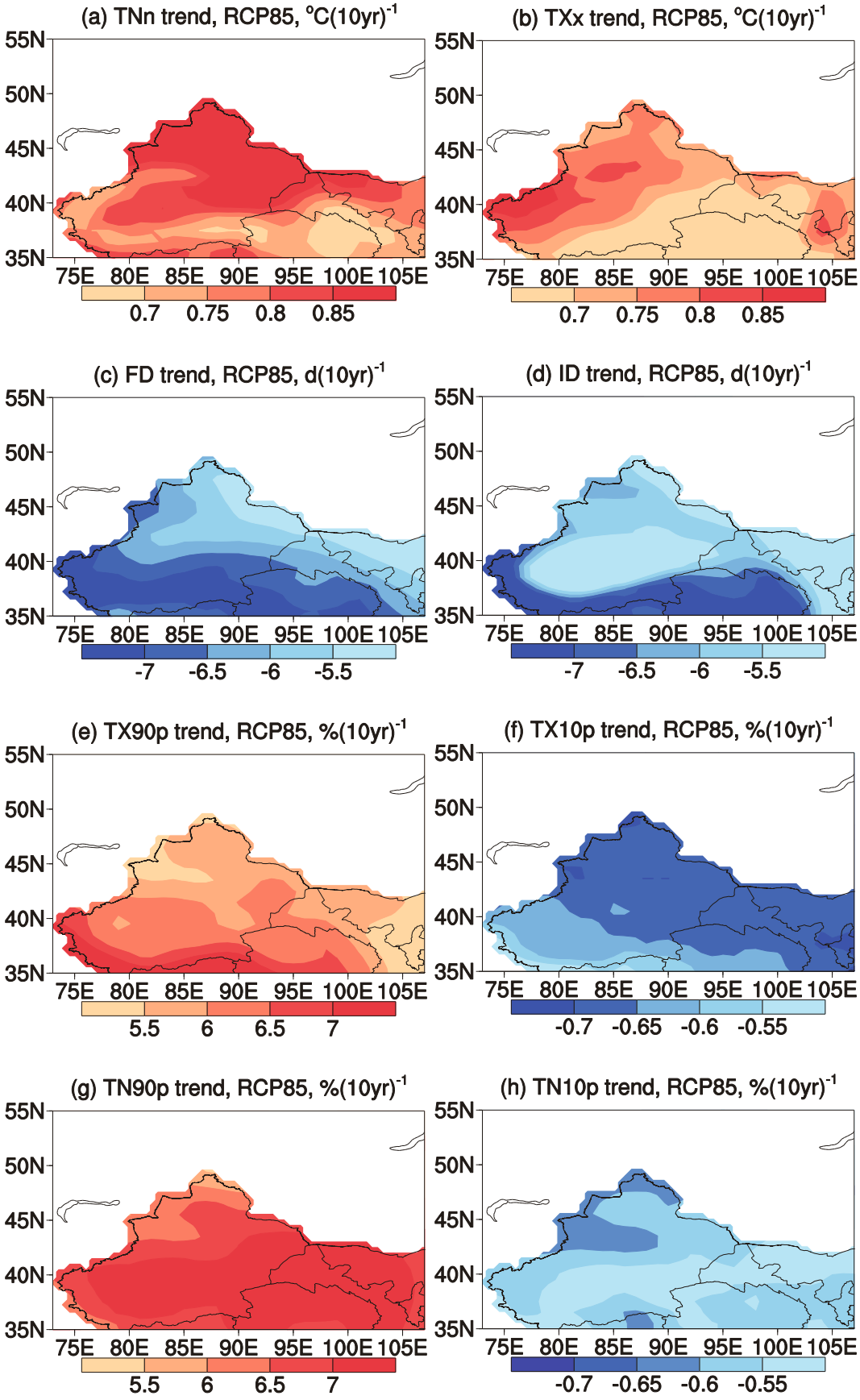

Fig. 9. The MME projected distribution of linear trends in temperature during 2020–99 under the RCP8.5 scenario.

der the RCP8.5 scenario (Fig. 9), the warming rates for TNn increase from south to north. For TXx, the increasing trend enlarges from southeast to northwest, with the most intense warming in western Xinjiang. The greatest decreases in FD and ID are projected to occur along the Kunlun Mountains, extending to Qinghai. The change in TX90p increases generally from northeast to southwest, while that in TX10p increases generally from southwest to northeast. The change in TN90p and TN10p is rather uniform across the region. The pattern under RCP4.5 presents a general resemblance to that under RCP8.5, albeit less pronounced than RCP8.5.

4.2. *Precipitation*

Figures 10a1–a5 display the MME-projected temporal changes of annual and seasonal mean precipitation averaged over the arid region of northwestern China under the RCP4.5 and RCP8.5 scenarios. All figures show a tendency toward an increase, with the rate being greater under RCP8.5 than RCP4.5, except in summer. Precipitation is projected to increase by 38.8 mm, 13.1 mm, 10.6 mm, 8.7 mm and 6.4 mm (34.9 mm, 12.4 mm, 9.2 mm, 7.9 mm and 5.3 mm) before the middle of this century, and by 77.2 mm, 28.9 mm, 16.2 mm, 18.0 mm and 14.3 mm (50.6 mm, 18.6 mm, 13.4 mm, 11.0 mm and 7.8 mm) at the end of this century, under the RCP8.5 (RCP4.5) scenario, compared with 1986–2005, for the annual mean and the spring, summer, autumn and winter seasons, respectively. Regionally, the southern part is expected to exhibit a larger rate of increase of annual mean precipitation than the northern part under the RCP8.5 scenario (Fig. 10c1). The distribution of linear trends in spring (Fig. 10c2) resembles that in winter (Fig. 10c5), with larger values appearing in the southern part and in northwestern Xinjiang. The pattern in summer (Fig. 10c3) is generally similar to that in autumn (Fig. 10c4), with a large increase in the southeastern part and a decrease in western Xinjiang. The distribution of precipitation change under RCP4.5 (Figs. 10b1–b5) resembles that under RCP8.5.

For precipitation extreme indices, increases in R95p (Fig. 11a1) and R1mm (Fig. 11a2) and decreases in CDD (Fig. 11a3) are projected in the 21st century. Relative to 1986–2005, R95p tends to increase by 17.3 mm and 50.9 mm (14.1 mm and 26.1 mm) under the RCP8.5 (RCP4.5) scenario by the middle and the end of this century, respectively. Their corresponding percentage changes are 24.3% and 71.5% (19.9% and 36.7%), larger than that for annual mean precipitation, which is 10.4% and 20.8% (9.3% and 13.6%), respectively. This hints at a disproportionally larger contribution from the increase of precipitation falling on very wet days to the total precipitation change. R1mm tends to increase by 3.3 days (2.6 days) before the middle of this century, and by 6.0 days (4.5 days) at the end of this century, under the RCP8.5 (RCP4.5) scenario. CCD is inclined to decrease by 5.4 days (4.7 days) before the middle of this century, and by 10.8 days (5.7 days) at the end of this century, under the RCP8.5 (RCP4.5) scenario. All the changes exceed the 95% significance level.

R95p is projected to increase across the region under the RCP8.5 scenario (Fig. 11c1). The spatial distribution of changes is generally similar to that of the annual precipitation, with the greatest increase occurring in the southern part of the region. This pattern again illustrates a greater contribution of extreme heavy precipitation to the enhancement of annual mean precipitation. The number of wet days is also projected to increase throughout the region, with the greatest changes in the southern and central part (Fig. 11c2). The maximum number of consecutive dry days (Fig. 11c3) is projected to decrease, particularly in Inner Mongolia and central Xinjiang. The pattern of the change under RCP4.5 (Figs. 11b1–b3) is similar to that under RCP8.5, but with weaker amplitude.

5. Conclusion

This study examined the changes of mean and extreme temperature and precipitation in the arid region of northwestern China since 1961, and projected their future changes during the 21st century under the RCP4.5 and RCP8.5 scenarios. The main conclusions are summarized as follows:

(1) The arid region has experienced apparent warming since the 1960s. Annual and seasonal mean temperatures all show an increasing tendency, and the warming in winter is the most pronounced. Significant and widespread warming is also apparent for the temperature extreme indices, such as increases in TNn and TXx, decreases in FD and ID, increases in TX90p and TN90p, and decreases in TX10p and TN10p. Moreover, the warming of the coldest night is larger than that of the warmest day, and the changes of cold and warm nights are more remarkable than those of cold and warm days.

(2) The annual and seasonal mean precipitation exhibit increasing trends. The annual precipitation amount in the last decade of the century is greater than in any preceding decade since 1961. R95p and R1mm also exhibit an increasing tendency, and CDD shows a tendency toward shorter durations of dry spells. Regionally, the annual mean precipitation increases across the entire region, except the western part of Inner Mongolia and the eastern corner of the region. The largest increases occur in Qinghai and the Tianshan Mountains region. The patterns of changes in R95p and R1mm are generally similar. The greatest increase is in Qinghai and northwestern Xinjiang; and there is a decrease in western Inner Mongolia and southern Gansu, which suggests that both extreme heavy precipitation and precipitation frequency play roles in increase or decreases of local precipitation amounts. In Ningxia and part of the Tarim Basin, precipitation frequency has a larger contribution to local precipitation change. CDD decreases particularly in eastern Xinjiang, western Gansu and northern Qinghai, while it increases in the western Tarim Basin, central and western Inner Mongolia, and southern Gansu.

(3) Continuous warming in temperature, concomitant with decreases in cold extremes and increases in warm extremes, is projected across the arid region, with greater change under RCP8.5 than under RCP4.5. For instance, com-

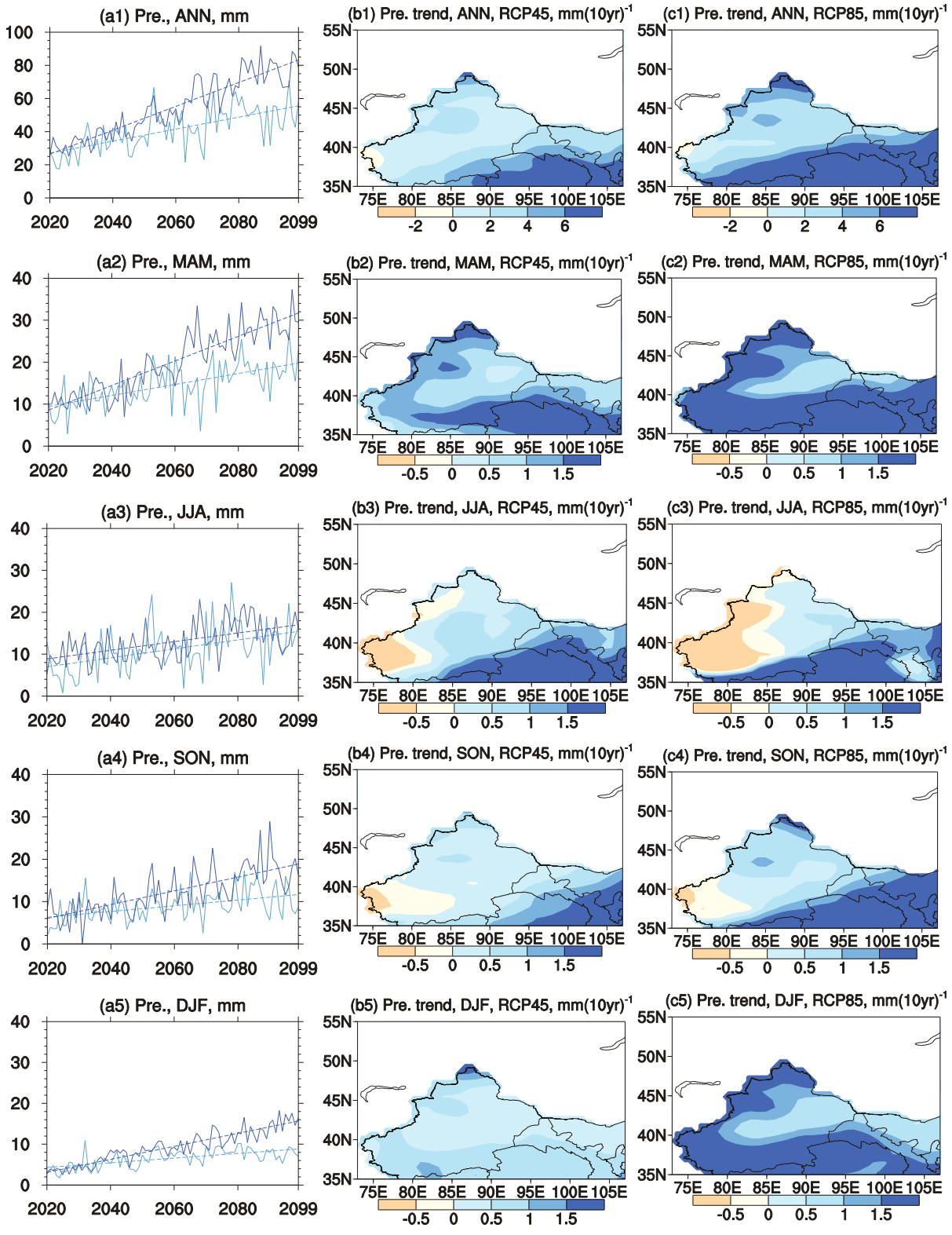

Fig. 10. The MME projected (a1–a5) temporal change of precipitation anomalies (relative to 1986–2005) averaged over the arid region of northwestern China under the RCP4.5 (light blue) and RCP8.5 (blue) scenarios, and spatial distribution of linear trends in precipitation during 2020–99 under (b1–b5) RCP4.5 and (c1–c5) RCP8.5. Dashed lines show linear trends.

pared with 1986–2005, under the RCP8.5 scenario and by the end of the 21st century, the annual mean temperature, TNn and TXx are projected to increase by 5.5°C, 6.6°C and 5.6°C, respectively; FD and ID are projected to decrease by 58 days and 47 days, respectively; TX90p and TN90p are projected to increase by 47.2% and 55.7%, respectively; and TX10p and

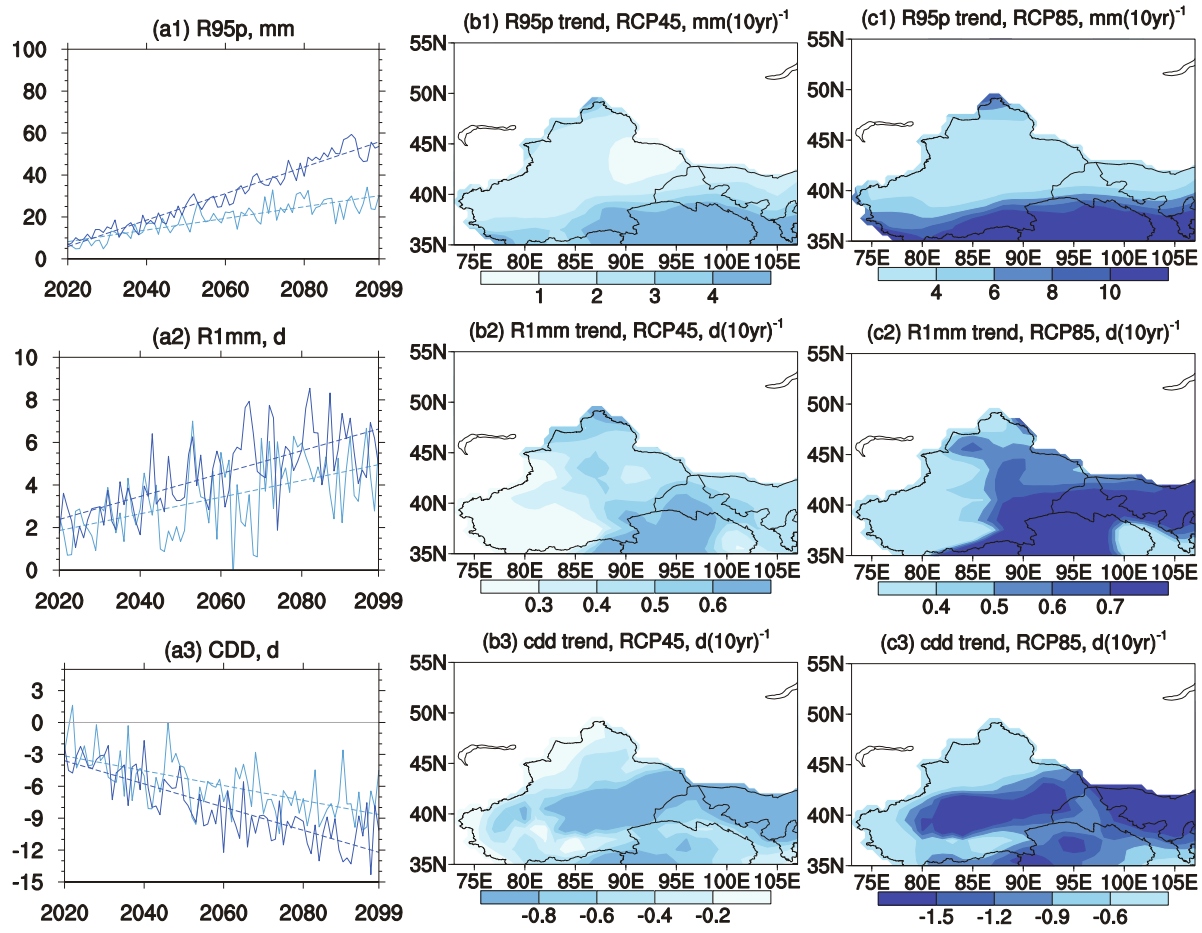

Fig. 11. The MME projected (a1–a3) temporal change of precipitation extreme indices averaged over the arid region of northwestern China under the RCP4.5 (light blue) and RCP8.5 (blue) scenarios, and spatial distribution of linear trends in precipitation during 2020–99 under (b1–b3) RCP4.5 and (c1–c3) RCP8.5. All indices are anomalies relative to 1986–2005. Dashed lines show linear trends.

TN10p are projected to decrease by 7.7% and 7.6%, respectively.

(4) A general intensification of precipitation is projected over the arid region. Relative to 1986–2005, the percentage changes in annual precipitation and R95 are projected to increase by 13.6% and 36.7% under the RCP4.5 scenario and by 20.8% and 71.5% under the RCP8.5 scenario, respectively, by the end of this century. The similar distribution of changes between R95p and annual precipitation, and the greater percentage change in R95p than in annual precipitation, reflect a greater contribution from the increase in extreme heavy precipitation to the total precipitation change. R1mm is also projected to increase, and CDD to decrease, across the entire region.

In this study, we used the period 1961–90 for the observational anomalies, while the typical period of 1986–2005 was used for the CMIP5 analysis. If the observational anomalies are relative to the reference period adopted for the CMIP5 analysis, similar results can be obtained. Besides, the projection reflects a possible estimate of the state-of-the-art climate models under warming scenarios. There are still uncertainties in the projection due to the uncertainty of forcing scenarios and climate models. Natural climate variability may also bring relevant uncertainty to the projected changes (Zhou et al., 2014).

Acknowledgements. We acknowledge the World Climate Research Program's Working Group on Coupled Modeling, which is responsible for CMIP, and thank climate modeling groups for producing and making available their model output. This research was jointly supported by the National Basic Research Program of China (Grant No. 2012CB955900), the National Key Research and Development Program of China (Grant No. 2016YFA0600701), and the National Natural Science Foundation of China (Grant No. 41675069).

REFERENCES

Alexander, L. V., and J. M. Arblaster, 2009: Assessing trends in observed and modelled climate extremes over Australia in relation to future projections. *International Journal of Climatology*, **29**, 417–435.

Alexander, L. V., and Coauthors, 2006: Global observed changes

in daily climate extremes of temperature and precipitation. *J. Geophys. Res*., **111**, D05109, doi: 10.1029/2005JD006290.

Chen, H. P., 2013: Projected change in extreme rainfall events in China by the end of the 21st century using CMIP5 models. *Chinese Science Bulletin*, **58**, 1462–1472, doi: 10.1007/s11434-012-5612-2.

Donat, M. G., and Coauthors, 2013: Updated analyses of temperature and precipitation extreme indices since the beginning of the twentieth century: The HadEX2 dataset. *J. Geophys. Res*., **118**, 2098–2118.

Gao, X. J., Z. C. Zhao, and Y. H. Ding, 2003: Climate change due to greenhouse effects in northwest China as simulated by a regional climate model. *Journal of Glaciology and Geocryology*, **25**(2), 165–169. (in Chinese with English abstract)

Gao, X. J., J. S. Pal, and F. Giorgi, 2006: Projected changes in mean and extreme precipitation over the Mediterranean region from a high resolution double nested RCM simulation. *Geophys. Res. Lett*., **33**, L03706, doi: 10.1029/2005GL024954.

Gao, X. J., M. L. Wang, and F. Giorgi, 2013: Climate change over China in the 21st century as simulated by BCC_CSM1.1-RegCM4.0. *Atmospheric and Oceanic Science Letters*, **6**(5), 381–386.

Gleckler, P. J., K. E. Taylor, and C. Doutriaux, 2008: Performance metrics for climate models. *J. Geophys. Res*., **113**, D06104, doi: 10.1029/2007JD008972.

Gupta, A. S., N. C. Jourdain, J. N. Brown, and D. Monselesan, 2013: Climate drift in the CMIP5 models. *J. Climate*, **26**, 8597–8615.

Huang, J. P., J. J. Ran, and M. X. Ji, 2014: Preliminary analysis of the flood disaster over the arid and semi-arid regions in China. *Acta Meteorologica Sinica*, **72**(6), 1096–1107. (in Chinese with English abstract)

IPCC, 2013: *Climate Change 2013: The Physical Science Basis*. *Contribution of Working Group I to the Fifth Assessment Report of the Intergovernmental Panel on Climate Change*. Cambridge University Press, Cambridge, United Kingdom and New York, NY, USA, 1535 pp.

Ji, Z. M., and S. C. Kang, 2013a: Projection of snow cover changes over China under RCP scenarios. *Climate Dyn*., **41**, 589–600.

Ji, Z. M., and S. C. Kang, 2013b: Double-nested dynamical downscaling experiments over the Tibetan Plateau and their projection of climate change under two RCP scenarios. *J. Atmos. Sci*., **70**, 1278–1290.

Ji, Z. M., and S. C. Kang, 2015: Evaluation of extreme climate events using a regional climate model for China. *International Journal of Climatology*, **35**, 888–902.

Jiang, D. B., M. F. Su, R. Q. Wei, and B. Liu, 2009a: Variation and projection of drought and wet conditions in Xinjiang. *Chinese Journal of Atmospheric Sciences*, **33**(1), 90–98. (in Chinese with English abstract)

Jiang, D. B., Y. Zhang, and J. Q. Sun, 2009b: Ensemble projection of 1–3° warming in China. *Chinese Science Bulletin*, **54**, 3326–3334.

Jiang, D. B., Z. P. Tian, and X. M. Lang, 2016: Reliability of climate models for China through the IPCC Third to Fifth Assessment Reports. *International Journal of Climatology*, **36**, 1114–1133.

Kharin, V. V., F. W. Zwiers, X. B. Zhang, and G. C. Hegerl, 2007: Changes in temperature and precipitation extremes in the IPCC ensemble of global coupled model simulations. *J. Climate*, **20**, 1419–1444.

Kruger, A. C., and S. S. Sekele, 2013: Trends in extreme temperature indices in South Africa: 1962–2009. *International Journal of Climatology*, **33**, 661–676.

Li, J., Q. He, J. Q. Yao, and W. F. Hu, 2014: The characteristics of climate change and the impact factors analysis in the western part of Inner Mongolia. *Journal of Arid Land Resources and Environment*, **28**(5), 186–191. (in Chinese with English abstract)

Liu, S. Y., Y. J. Ding, Y. Zhang, D. H. Shangguan, J. Li, H. D. Han, J. Wang, and C. W. Xie, 2006: Impact of the glacial change on water resources in the Tarim River Basin. *Acta Geographic Sinica*, **61**(5), 482–490. (in Chinese with English abstract)

Ren, Z. X., and D. Y. Yang, 2006: Study on the division and trends of temperature variation in Northwest arid area of China in recent 50 Years. *Journal of Arid Land Resources and Environment*, **20**(1), 99–103. (in Chinese with English abstract)

Rusticucci, M., 2012: Observed and simulated variability of extreme temperature events over South America. *Atmospheric Research*, **106**, 1–17.

Shi, Y. F., and J. Zhao, 2014: Study on spatial-temporal characteristics of extreme temperature in arid areas of Northwest China. *Journal of Lanzhou University* (*Natural Sciences*), **50**(4), 529–533. (in Chinese with English abstract)

Shi, Y. F., Y. P. Shen, and R. J. Hu, 2002: Preliminary study on signal, impact and foreground of climatic shift from warm-dry to warm-humid in Northwest China. *Journal of Glaciology and Geocryology*, **24**(3), 219–226. (in Chinese with English abstract)

Sillmann, J., V. V. Kharin, F. W. Zwiers, X. Zhang, and D. Bronaugh, 2013: Climate extremes indices in the CMIP5 multimodel ensemble: Part 2. Future climate projections. *J. Geophys. Res*., **118**, 2473–2493.

Song, L. C., and C. J. Zhang, 2003: Changing features of precipitation over Northwest China during the 20th century. *Journal of Glaciology and Geocryology*, **25**(2), 143–148. (in Chinese with English abstract)

Taylor, K. E., R. J. Stouffer, and G. A. Meehl, 2012: An overview of CMIP5 and the experiment design. *Bull. Am. Meteor. Soc*., **93**, 485–498.

Tebaldi, C., K. Hayhoe, J. M. Arblaster, and G. A. Meehl, 2006: Going to extremes: An intercomparison of model-simulated historical and future changes in extreme events. *Climatic Change*, **79**, 185–211.

Wu, J., and X. J. Gao, 2013: A gridded daily observation dataset over China region and comparison with the other datasets. *Chinese Journal of Geophysics*, **56**(4), 1102–1111. (in Chinese with English abstract)

Wu, J., X. J. Gao, Y. Shi, and F. Giorgi, 2011: Climate change over Xinjiang region in the 21st century simulated by a high resolution regional climate model. *Journal of Glaciology and Geocryology*, **33**(3), 479–487. (in Chinese with English abstract)

Xu, C. H., Y. Xu, and Y. Luo, 2008: Climate change of the 21st century in Xinjiang with SRES scenarios. *Desert and Oasis Meteorology*, **2**(3), 1–7. (in Chinese with English abstract)

Xu, J. Y., Y. Shi, and X. J. Gao, 2012: Changes in extreme events as simulated by a high-resolution regional climate model for the next 20–30 years over China. *Atmospheric and Oceanic Science Letters*, **5**(6), 483–488.

Xu, Y., and C. H. Xu, 2012: Preliminary assessment of simulations of climate changes over China by CMIP5 multi-models. *Atmospheric and Oceanic Science Letters*, **5**, 489–494.

Xu, Y., Y. H. Ding, and Z. C. Zhao, 2003: Scenario of tempera-

ture and precipitation changes in Northwest China due to human activity in the 21st century. *Journal of Glaciology and Geocryology*, **25**(3), 327–330. (in Chinese with English abstract)

Zhang, Q., Y. Q. Hu, X. Y. Cao, and W. M. Liu, 2000: On some problems of arid climate system of Northwest China. *Journal of Desert Research*, **20**(4), 357–362. (in Chinese with English abstract)

Zhang, X. B., L. Alexander, G. C. Hegerl, P. Jones, A. K. Tank, T. C. Peterson, B. Trewin, and F. W. Zwiers, 2011: Indices for monitoring changes in extremes based on daily temperature and precipitation data. *WIREs Climate Change*, **2**, 851–870.

Zhou, B. T., Q. H. Wen, Y. Xu, L. C. Song, and X. B. Zhang, 2014: Projected changes in temperature and precipitation extremes in China by the CMIP5 multimodel ensembles. *J. Climate*, **27**, 6591–6611.

Zhou, B. T., Y. Xu, J. Wu, S. Y. Dong, and Y. Shi, 2016: Changes in temperature and precipitation extreme indices over China: Analysis of a high-resolution grid dataset. *International Journal of Climatology*, **36**, 1051–1066.